

The group of galaxies around 3C 275.1

J. Krempeć-Krygier¹, B. Krygier², and G. Walentynowicz²

¹ N. Copernicus Astronomical Center, Astrophysical Lab., Toruń, Poland

² Toruń Centre for Astronomy, Toruń, Poland

Received 23 April 1997 / Accepted 28 January 1998

Abstract. We have found that the quasar 3C275.1 is located at the centre of the gravitational well of a group of galaxies characterized by relativistic radial velocity and velocity dispersion equal to 124414 and 297 km s⁻¹ respectively.

The temperature of the ICM gas calculated from the „ β ” model is about $6.7 \cdot 10^6$ K. We suggest that there is a cooling flow in the ICM at a deposition rate of about $140 M_{\odot} \text{yr}^{-1}$. It supplies gas to the narrow-emission line region, in which the number density is equal to 0.4 and 2.3cm^{-3} for homogeneous region and clouds of radii of 10 kpc respectively. The 1.6 GHz European VLBI Network image of the quasar core shows the elongation of radio structure at a distance ~ 40 mas from the core with a position angle about 255° . It may be the result of interactions between out-flowing plasma of the QSO and the nonuniform ionized gas emitting in forbidden [OII] and [OIII] emission lines. The non-collinearity of the radio structure of 3C 275.1 might be explained by an oblique shock of the plasma jet at the interface with the halo of a neighbouring galaxy or with clouds of ionized gas.

Key words: galaxies: clusters: individual: A 98 – quasars: individual: 3C 275.1 – cooling flows – galaxies: jets – intergalactic medium – radio continuum: galaxies

1. Introduction

Active galactic nuclei (AGN) in rich clusters of galaxies evolve faster than those in poor environments. The nearby clusters of galaxies usually contain radio weak galaxies of the Fanaroff-Riley I (FRI) type, while quasars at low redshifts ($z \leq 0.5$) rarely, if ever, occur in rich clusters of galaxies (Stockton, 1980). On the other hand, the radio-loud quasars with $z \geq 0.5$ are often found in rich clusters. The time scales of evolution of AGN activity are similar to the dynamical ones of clusters of galaxies. Therefore, only the dynamical evolution of cluster cores may be responsible for the evolution of AGN at these time scales. The virialisation of cluster core increases the galaxy velocities in the core up to the values, where the galaxy-galaxy interactions are not effective enough to stop AGN activity. Then, the galaxy

velocities in the vicinity of those AGNs (mainly quasars) are rather low.

The aim of the paper is to find the mechanism responsible for the non-collinearity of the radio structure of radio-loud quasar (RLQSO) 3C 275.1. Therefore, in Sect. 2 we shall discuss the dynamics of a group of galaxies around it to see if the drag force due to the motion of the host galaxy through the intracluster medium (ICM) could cause the bending of the radio jet.

On the other hand it is known that RLQSOs are stronger sources of X-ray emission than the radio-weak ones (Wilkes et al. 1994). Their X-ray emission, if spatially resolved, usually consists of the point-like emission of the QSO itself and of extended emission from the hot intra-cluster gas. It has been argued from both the theoretical and an observational standpoint that the X-ray gas in the cores of galaxy clusters or groups can cool and accrete onto the slow moving dominant galaxy. Thermal instabilities in the in-flowing gas are thought to cause cooling of dense knots, which are identified with the optical emission-line filaments seen around the dominant cluster galaxies. Since 3C 275.1 exhibits one of the largest and most luminous extended emission-line regions (Hintzen and Stocke, 1986) it lies in a cooling accretion flow. Its extended narrow-line emission nebula and the X-ray emission will also be discussed in Sect. 2. We shall derive the temperature of the gas emitting in X-rays and the accretion mass deposition rate as well as particle number density in narrow-emission line region.

In Sect. 3 we shall discuss the radio structure of 3C 275.1 and the oblique shocks to explain its non-collinearity. A 1.6 GHz European VLBI Network image of the quasar core will be presented in Appendix C. We assume the Hubble constant $H_0 = 50 \cdot h \text{ km (s Mpc)}^{-1}$ and $q_0 = 0.5$ throughout this paper. Then, at the distance of 3C 275.1 ($z = 0.5549$), 1 arcsec corresponds to $7.44 h^{-1} \text{ kpc}$ and the luminosity distance is $d_L = 3695 h^{-1} \text{ Mpc}$.

2. Properties of the group of galaxies and extended narrow- emission line nebula

3C 275.1 (1241+166) was the first quasar found at the centre of rich cluster of galaxies (Hintzen and Stocke 1986). The galaxy field around 3C 275.1 has been investigated by Hintzen et al. (1981), Hintzen (1984) and Ellingson and Yee (1994). They

have found an excess of galaxies around it and have measured the redshifts of the number of galaxies. We have used these redshifts to discuss the dynamics of galaxies in the vicinity of 3C 275.1. The comparison of redshifts estimated by Hintzen and Ellingson and Yee indicates that they agree well with the exception of 3C 275.1-2=381. Since Hintzen (1984) determined redshift of this galaxy using four spectral lines, while Ellingson and Yee only from one line, we have taken his redshift. For all galaxies we have calculated the relativistic radial velocities

$$V_r = c \cdot \frac{[(1+z)^2 - 1]}{[(1+z)^2 + 1]}.$$

To remove non-cluster galaxies we have applied the „ $3\text{-}\sigma$ ” procedure described by Yahil and Vidal (1977). Accordingly, all galaxies with velocities more than $3 \cdot \sigma_{cl}$ away from the central velocity have been rejected. The process was repeated until we obtain a stable number of galaxies, namely 6 galaxies given in Table 1.

These galaxies belong to a group dynamically bound to the quasar. We have calculated the relativistic radial velocity of the group V_r^{cl} and the velocity dispersion σ_{cl} , which are 124414 ± 86 and 297 km s^{-1} respectively. Assuming a radius for the group of galaxies equal to $2.3'$, which corresponds to $R_A = 1.02 h^{-1} \text{ Mpc}$, and the optical position of the host galaxy of 3C 275.1 to be the group center, we derived the distances of the galaxies from this center „ d ”, the distances in respect to the group radius „ $\frac{d}{R_A}$ ” and the position angles measured from the north towards the east „ PA ”.

In Table 1 the names of galaxies, their redshifts, the calculated relativistic radial velocities, the relativistically corrected differences of radial velocities,

$$\Delta V_r = \frac{V_r - V_r^{cl}}{1+z}$$

the distances „ R ” and the projected distances „ R_g ” from the core (see Sect. 3) are given. The relative errors of radial velocities estimated from the measured accuracy of redshifts are smaller than 0.14 %. We find that the host galaxy of 3C 275.1 with its $\Delta V_r = -39 \text{ km s}^{-1}$ (see Table 1) lies at the centre of the gravitational well of the group.

We have also applied the biweight estimators described by Beers et al. (1990). Thereafter, we have determined the biweight location C_{BI} and the scale S_{BI} for galaxy velocities in the group. It is known that C_{BI} and S_{BI} are good estimators for Gaussian as well as non-Gaussian distributions. They become superior when only few galaxies are involved as in the case of 3C 275.1. We have derived 124378 km s^{-1} and 529 km s^{-1} for C_{BI} and S_{BI} respectively. Therefore, C_{BI} agrees with V_r^{cl} within the standard deviation. That confirms our earlier suggestion that the host galaxy of 3C 275.1 lies at the bottom of gravitational potential well of the group.

Recently, Rector et al. (1996) discussed the relation between the quasar-galaxy spatial covariance amplitudes B_{gq} and the radio morphological characteristics of radio sources in clusters of galaxies including 3C 275.1. In the sample analyzed, B_{gq} for the field of galaxies around 3C 275.1 has the highest value, i.e. 1125 ± 399 , which contradicts the six galaxies considered by

us as members of the group. The whole sample discussed by Ellingson et al. (1994) consists of 71 galaxies, which might be members of the group of galaxies around 3C 275.1 on the basis of the commonly used $m_3 \pm 3^m$ criterion. Here m_3 is the apparent brightness of the third bright galaxy in the cluster. Our analysis confirms how misleading such a membership criterion may be, particularly for distant clusters of galaxies. We have discovered a foreground group of galaxies at $z \approx 0.46$ containing >40 galaxies, which is not dynamically bound with the group around 3C 275.1. On the other hand, the amplitude of the angular covariance function is only 0.60 for the whole field, namely for the sphere of radius 3.52 . The amplitudes of the spatial correlation function are always <100 .

We derived the cluster dynamical time, defined as $t_d^{cl} = \frac{R_A}{\sigma_{cl}}$, and the galactic dynamical time ($t_d^{gal} = \frac{R_{gal}}{\sigma_{gal}}$) of the order of $2 \cdot 10^9$ yrs and $1.6 \cdot 10^8$ yrs respectively for $R_{gal} = 52.08 \text{ kpc}$ and $\sigma_{gal} = 200 \text{ km s}^{-1}$. Moreover, there is 381 galaxy at a distance of only $6.''7$ from the quasar. It lies along the direction (within the possible estimation error) of the NW lobe and the core of 3C 275.1. The impact of the radio jet on its halo might result in the formation of an oblique shock and cause the non-collinearity of the radio structure. We shall discuss this in Sect. 3.

The host galaxy of 3C 275.1 ($M_r = -24.{}^m9$) is similar to cD galaxies in nearby clusters of galaxies. The elliptical nebulosity, which is centered on the quasar, extends from the north-east towards the south-west at position angle about 40° and measures $14'' \times 7''$ (i.e. $104 \times 52 \text{ kpc}$) in the R-photometric system. In the V - photometric system only the stellar nucleus of the QSO is seen.

Now, we shall use the X-ray observations of 3C 275.1 and narrow-emission line measurements to determine the particle number densities. The Einstein IPC observation indicated that the QSO, group, or both are strong X-ray sources: $L_x = (3.6 \pm 1.5) \cdot 10^{44} \text{ ergs s}^{-1}$ in the $(0.5 \div 4.5) \text{ keV}$ band (Tananbaum et al., 1979). Since the X-ray source is marginally resolved, $\sim 1'$ in size, the observed X-ray flux may be due to either the quasar itself, to a cooling flow, or both. Based upon the PSPC observations with the ROSAT in the observed $(0.1 \div 2.4) \text{ keV}$ band ($(0.16 \div 3.73) \text{ keV}$ in the rest frame of QSO), Arp (1996) fitted a Raymond-Smith spectrum of temperature $T_{gas}^x = 1.6 \cdot 10^6 \text{ K}$ and Galactic neutral hydrogen column density of $N_H = 1.1 \cdot 10^{20} \text{ cm}^{-2}$ as well as a simple power-law with an energy photon index $\alpha = 1.93_{-0.08}^{+0.03}$ modified at low energy by photo-electric absorption in a uniform column density $N_H = 3.5 \cdot 10^{20} \text{ cm}^{-2}$ of cold gas.

On the other hand, from the HI observations at 21 cm by Stark et al. (1992) we estimate $N_H = 1.8 \cdot 10^{20} \text{ atoms} \cdot \text{cm}^{-2}$, which is intermediate between two above quoted values. The accuracy of the observations leads to N_H between 1.3 and $2.5 \cdot 10^{20} \text{ cm}^{-2}$. Therefore, it seems that above mentioned three values of hydrogen number density differ only marginally. It is worth noting that measured X-ray emission is significantly extended (about $83''$) and might be emitted by hot gas of the cooling flow. Furthermore, an upper limit for the temperature of the ICM gas T_g^x can be derived from the equilibrium condi-

Table 1. Dynamical data for group of galaxies around 3C 275.1

Name	z	$V_r \pm \sigma$ [km/s]	ΔV_r [km/s]	d [arcsec]	$\frac{d}{R_A}$	PA [deg]	R [Mpc]	R_g [kpc]
3C 275.1	0.5549	124358 ± 90	-39	0	0	–	0.00	0.00
381	0.5539	124198 ± 180	-152	6.7	0.05	156	-1.01	49.85
3C 275.1-7	0.5535	124134 ± 90	-197	25	0.18	186	-1.31	185.93
464	0.5563	124581 ± 90	+119	63	0.46	21	+1.41	468.99
450	0.5544	124278 ± 112	-96	77	0.56	15	-0.50	572.64
248	0.5585	124931 ± 89	+366	136	0.99	198	+3.60	1014.58

tion between the kinetic energy of the group of galaxies and the thermal gas energy, i.e.

$$k \cdot T_g^x = \mu \cdot m_p \cdot \sigma_{cl}^2$$

(here $m_p = 1.67 \cdot 10^{-24}$ g is the proton mass, μ -the mean molecular weight). Simulations of X-ray clusters by Navarro et al. (1995) indicate that this condition is fulfilled moderately well by the „ β -model” over all but the innermost regions. Putting for the solar abundances $\mu = 0.63$ (Edge & Stewart, 1991) and the velocity dispersion of the group of galaxies $\sigma_{cl} = 297 \text{ km} \cdot \text{s}^{-1}$ (see Table 1), we derived $T_g^x = 6.7 \cdot 10^6$ K, while for $\mu = 1$ the upper limit for the gas temperature is about $1.1 \cdot 10^7$ K. In further calculations we take T_g^x for $\mu = 0.63$. Such a cool ($T \approx \text{few } 10^6$ K) gas is characteristic of cooling flows. The calculated temperature refers to the whole group of galaxies, while the temperature $T_{gas}^x = 1.6 \cdot 10^6$ K might occur in the central region of the group, where cooling flow appears. In the standard picture of cooling flows (Fabian et al., 1984, 1991; Sarazin, 1986) as the hot gas cools through 10^6 K and condenses, it will emit EUV and soft X-ray radiation, which can photoionize the previously condensed cooler denser matter and fuel an optical emission-line spectrum.

We derive the lower limit on the number density of the ICM gas from the condition that the cooling time t_c should be shorter than the Hubble time t_H . The present Hubble time is given by $t_H(o) = \frac{2}{3 \cdot H_0} = 1.3 \cdot 10^{10}$ yrs. The Hubble time at the redshift of 3C 275.1 is $t_H(0.5549) = t_H(o) \cdot (1+z)^{-1.5} = 6.7 \cdot 10^9$ yrs, while the cooling time scale is defined as $t_c = \frac{5kT}{n\Lambda}$ (where n is the number density and Λ -the standard cooling function or the volume emissivity). In the temperature range $10^5 \leq T \leq 10^7$ K, the numerical calculations indicate

$$\Lambda = (3 \cdot 10^{-23}) \cdot \left(\frac{T}{10^7}\right)^{-0.5} \text{ergs cm}^3 \text{s}^{-1}$$

(Raymond & Smith, 1977). Therefore, the lower limit on the number density of ICM gas is given by:

$$n_{ICM} \geq \frac{5 \cdot k \cdot T}{t_c \cdot \Lambda}$$

For $T_g^x = 6.7 \cdot 10^6$ K and $t_H(0.5549)$ we have calculated $n_{ICM} \geq 5.97 \cdot 10^{-4} \text{ cm}^{-3}$.

It seems that accreting matter from a cluster cooling flow of the type seen in low-redshift clusters, which are X-ray sources (Stewart et al., 1984) is the material in the nebosity. Hutchings (1992) found that extended emission structure occurs in

all RLQSOs discussed with a variety of properties and z from 0.36 to 0.91. However, it is generally stronger in the large lobe-dominated (steep spectrum) sources, such as 3C 275.1, than in compact (flat spectrum) ones.

Crawford and Fabian (1989) have obtained the narrow-band images of 3C 275.1 along the major axis of the elliptical nebosity centered on the quasar in the O[III] $\lambda = 500.7$ nm and [OII] $\lambda = 372.7$ nm emission lines redshifted to 778.6 nm and 579.6 nm respectively as well as in a nearby line-free continuum band. They have found that the narrow emission lines of [OII] and [OIII] extend well into the nebosity on either side of the nucleus up to $6''5$ in NE and about $6''$ in SW directions. The upper limit on the number density of the cooler extended and denser emission line gas is determined by the pressure equilibrium with the ICM gas (Stockton & Mac Kenty 1987). In the other case, the cooler gas having $T_{em} \approx 10^4$ K, which should be accurate to a factor of 2, contained within the radius of 52 kpc will disperse at its internal sound speed $c_s \approx \left(\frac{3 \cdot k \cdot T_{em}}{m_p}\right)^{0.5}$, i.e. about $16 \text{ km} \cdot \text{s}^{-1}$ during the acoustic time scale $t_s = 1.4 \cdot 10^{10} \cdot r \cdot (T_{em})^{-0.5}$, i.e. $7 \cdot 10^9$ yrs, where „ r ” is the radius of the ENLR in kpc. The acoustic time scale is comparable with the Hubble time for $z=0.5549$. Therefore, from the pressure equilibrium condition we obtain

$$n_{ext} = n_{em} \geq n_{ICM} \frac{T_g^x}{T_{em}}$$

which gives 0.4 cm^{-3} ($\rho_{ext} = n \cdot m_H \approx 6.7 \cdot 10^{-26} \text{ g} \cdot \text{cm}^{-3}$) for $T_g^x = 6.7 \cdot 10^6$ K and $T_{em} \approx 1.0 \cdot 10^4$ K. The cooling time will be shorter and number density greater for central regions of the nebosity.

However, Hintzen and Romanishin (1986) found that the narrow-emission nebula displays considerable structure. There are several knots each with luminosity of $L_{[OII]} = 3.7 \cdot 10^{41} \text{ ergs} \cdot \text{s}^{-1}$, while the total [OII] luminosity is about $6.2 \cdot 10^{42} \text{ ergs} \cdot \text{s}^{-1}$ (Hes et al., 1993). Hence, inhomogeneous cooling might occur in 3C 275.1 similar to that observed in some nearby clusters of galaxies (Prestwich et al., 1995). We shall calculate the particle number density in such knots. The condensates will cool isobarically, while the dynamical time is smaller than the cooling one, which is fulfilled. As a dynamical time we consider the time required for a sound wave to cross the cooling cloud, i.e. $t_d = N_F \cdot P^{-1} \cdot (m_{av} \cdot kT)^{0.5}$. Here P is the pressure of the cloud gas and m_{av} -the mean mass per particle.

For the mean molecular weight above mentioned $\mu = 0.63$, we have $m_{av} = \mu \cdot m_H$. This condition implies an upper limit on the column density of particles in such a condensate/or cloud, namely

$$N_F \leq 2 \cdot 10^{21} \cdot \left(\frac{T}{10^7}\right)^2 \text{cm}^{-2},$$

which gives about $2 \cdot 10^{20} \text{cm}^{-2}$. However, some clouds will evaporate. The thermal condition and the limitation on the clouds which survive are

$$N_c \approx \left(\frac{\kappa \cdot T}{\Lambda}\right)^{0.5},$$

where κ is the standard conduction coefficient given by

$$\kappa = 5.6 \cdot 10^{-7} \cdot T^{2.5} \text{ergs s}^{-1} \text{K}^{-1} \text{cm}^{-1}$$

(Böhringer & Fabian, 1989). Putting $T = 6.7 \cdot 10^6 \text{K}$ we calculate $N_c \geq 9 \cdot 10^{19} \text{cm}^{-2}$. Therefore, the condensing clouds might contain particle number densities between N_c and N_F , namely about 10^{20} particles per cm^2 . On the other hand, the critical density of the particle will be determined by self-gravitation. The condensations will survive, when $t_c^g \leq t_{ff}$ in the potential well, i.e. roughly when the inflow velocity approaches the sound velocity. Here, t_{ff} is the free-fall time. For $T_g^x \approx 10^7 \text{K}$, we have $t_c^g(r \leq 10 \text{kpc}) \approx t_{ff}$, and thermal instabilities ought to develop. The gas will continue to flow into the central region and condense until self-gravitation induces clouds to coalesce and collapse. Self-gravitation will begin to dominate cloud dynamics at a total density larger than

$$N_{cr} = \left(\frac{P}{(\pi \cdot G \cdot m_{av}^2)}\right)^{0.5} \approx (7 \cdot 10^{22}) \cdot P_{-9}^2$$

regardless of the temperature of the inter-cloud gas. Here P_{-9} is the pressure of intra-cloud gas given in $10^{-9} \text{dyn cm}^{-2}$ scale and m_{av} -mean mass per particle. Putting $P_{-9} = 0.31$ we derived $N_{cr} = 7 \cdot 10^{21} \text{cm}^{-2}$ and the critical number density $n_{cr}(r \leq 10 \text{kpc}) \approx 2.3 \text{cm}^{-3}$ ($\rho_{cr} \approx 3.84 \cdot 10^{-24} \text{gcm}^{-3}$), which is about a factor 6 larger than n_{ext} calculated above. Hence, self-gravitation will be insignificant for narrow-emission line clouds of 3C 275.1. Pinkney et al. (1996) and Wilson (1992) discussed the connections between the radio structure and the emission in forbidden-narrow lines. Jets might also be deflected by clouds in ENLR as previously mentioned. The gas emitting in the outskirts of radio lobes could form an irregular „Faraday screen” and be responsible for depolarization of the radio emission. Such depolarization is observed, especially in the SE lobe.

The narrow-emission line spectra are typically reproducible by photo-ionization by a relatively dilute power-law continuum. Hence, knowing the changes of the narrow-emission line ratios, namely $[\text{OIII}]\lambda = 500.7 \text{nm}/[\text{OII}]\lambda = 372.7 \text{nm}$, with distance from the nucleus and assuming photo-ionization by the QSO core, the pressure profiles of the gas can be deduced (Crawford and Fabian 1989). However, to estimate the ionizing luminosity, the X-ray luminosity of the QSO must be known. To derive the minimum pressure for the line emitting gas a power law between the optical and X-ray wave-bands has been assumed and the spectral index $\alpha_{ox} = 1.22$ has been taken from Worrall et al., 1987. Hence, the power-law luminosity is $3.3 \cdot 10^{55} \text{ph s}^{-1}$,

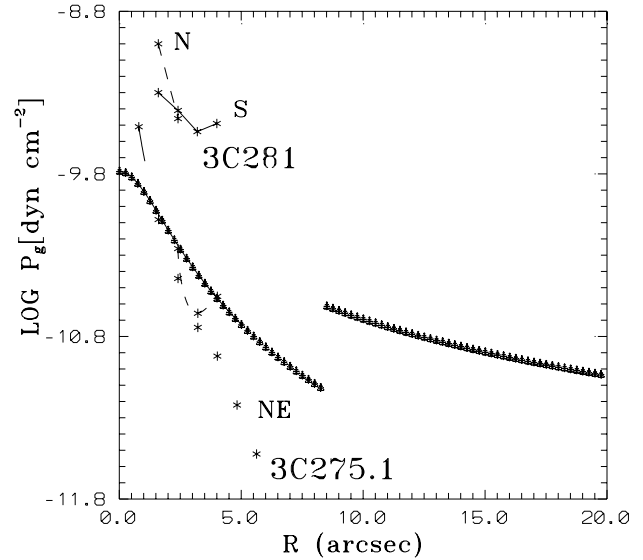


Fig. 1. Changes of thermal pressure of narrow-emission gas with distance along the major axis of 3C 275.1 ($z=0.5549$) and 3C281 ($z=0.599$). Changes of the pressure of ICM gas for $a_c = 250 \text{kpc}$ and $p_0 = 1.0 \cdot 10^{-11} \text{dyn cm}^{-2}$ are superimposed.

which is a little lower than is typical $(4 \pm 2) \cdot 10^{56} \text{ph s}^{-1}$ for the „ $z \approx 1$ ” QSOs. In Fig. 1 the pressure profiles of the ionized gas for 3C 275.1 and 3C281 ($z=0.599$) (Crawford et al., 1991)-a QSO almost at the same distance as 3C 275.1 and also lying in a group of galaxies (Yee & Green, 1987) are compared with changes of the pressure of the ICM gas. The changes of the pressure of the ICM gas with distance are described by “ β -model, i.e. $P_g^{ICM} = P_o \cdot (1 + (\frac{r}{a_c})^2)^{-1.5 \cdot \beta_r}$ for smaller distances and $P_g^{ICM} = P_o \cdot (1 + (\frac{r}{a_c})^2)^{-\beta_r}$ for distant regions of the cluster. Here $P_o = n_o \cdot k T_g$ and β_r is the β -parameter. The central particle densities n_o have been calculated from the X-ray luminosities L_x and core radii a_c as given by $n_o = 4.315 \cdot (\frac{L_x}{a_c^3})^{0.5}$. We put $L_x = 3.6 \cdot 10^{44} \text{erg s}^{-1}$ and two values for a_c , namely $a_c = 250 \text{kpc}$ and 150kpc . The former one represents the typical core radius of cluster of galaxies, while latter refers to the radius of cooling flow region. Hence, we have $n_o = 1.204 \cdot 10^{-2} \text{cm}^{-3}$, $P_o = 1.01 \cdot 10^{-11} \text{dyn cm}^{-2}$ and $n_o = 2.59 \cdot 10^{-2} \text{cm}^{-3}$; $P_o = 2.81 \cdot 10^{-11} \text{dyn cm}^{-2}$ for $T_g = 6.1 \cdot 10^6 \text{K}$. The calculated gas pressure profile of ICM gas is shown in Fig. 1.

It is seen that the pressure of gas close to 3C 275.1 is lower than that around 3C281, which has a mass deposition rate $> 500 M_\odot \cdot \text{yr}^{-1}$ (Bremer et al., 1992). In general, the derived pressure profiles of the extended emission-line gas toward the north-east of 3C 275.1 are similar to those of groups of galaxies, e.g. MKW 4 or MKW 3s, and are lower than those of rich clusters of galaxies. However, extra ionization due to interaction with the radio plasma might be invoked especially for the SW side.

The rate of condensation of gas extending over a region of radius r_c at the center of a cluster is

$$\dot{M} = 8 \cdot P_{-9}^2 \cdot T_7^{-3} \cdot A_{-23} \cdot r_c^3$$

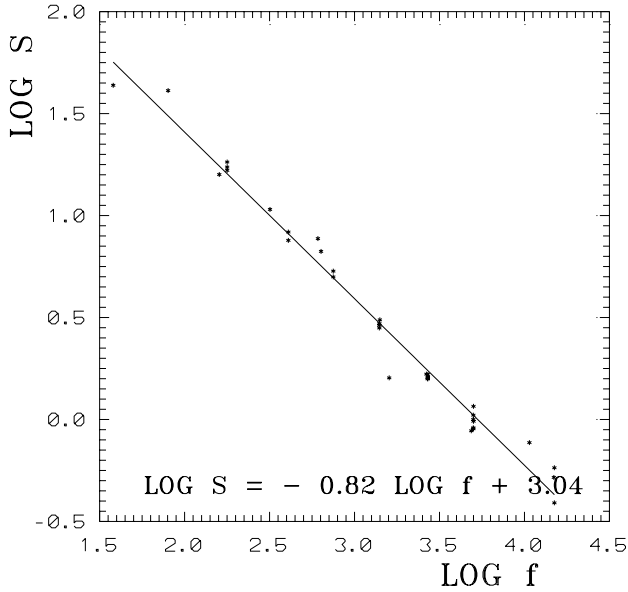


Fig. 2. Flux density – frequency relation

releasing a luminosity

$$L_c \approx 2 \cdot 10^{42} \cdot P_{-9}^2 \cdot T_7^{-2} \cdot \Lambda_{-23} \cdot r_c^3,$$

where $T_7 = T/10^7$ K and $\Lambda_{-23} = \Lambda/10^{-23} \text{erg} \cdot \text{cm}^3 \cdot \text{s}^{-1}$. Putting $r_c = 1''$ (7.44 kpc), $T_7 = 0.67$ K and $P_{-9} \approx 0.31 \text{dyn cm}^{-2}$ we calculate a condensation rate of about $140 M_\odot \text{yr}^{-1}$. The integrated mass deposition rates or condensation rates should be regarded as uncertain by (30 ÷ 50)%. Therefore, 3C 275.1 lies in a moderate cooling flow. Although no simple correlation between \dot{M} , t_c and optical line luminosity exists, Allen et al. (1995) showed that the most optically line-luminous clusters contain large cooling flows and exhibit short central cooling times of the order of a few $\cdot 10^8$ yrs.

3. Oblique shocks and non-collinearity of the radio structure of 3C 275.1

3C 275.1 (S(178 MHz)=11.4 Jy) exhibits significant non-collinearity of the radio structure (bending angle 23°) and belongs to the „dog-leg” QSOs. It has a straight steep spectrum between 0.02 and 15 GHz with $\alpha = 0.82$ and no sign of a low frequency turnover (see Fig. 2). The flux densities designated by stars in Appendix A are taken from ”A Catalogue of Radio Sources” by Kühr et al. (1979). They are on the absolute scale of Baars et al. (1977). The others are taken from papers quoted in Appendix A. The first radio observations with the Ryle 5 km radio telescope at 5 and 15 GHz (Jenkins et al. 1977, Riley and Pooley 1978) indicate that at 15 GHz 3C 275.1 consists of three components, namely a compact one, which coincides with the QSO, the slightly extended southern one at $6''$ and an unresolved component $9''$ north-west of the QSO, while at 5 GHz one component coincides with the north-west (NW) lobe and another one intermediate between the core and the south-east (SE) lobe.

VLA observations at 6 and 20 cm by Stocke et al. (1985) show a disturbed „bridge” extended back from the edge bright-

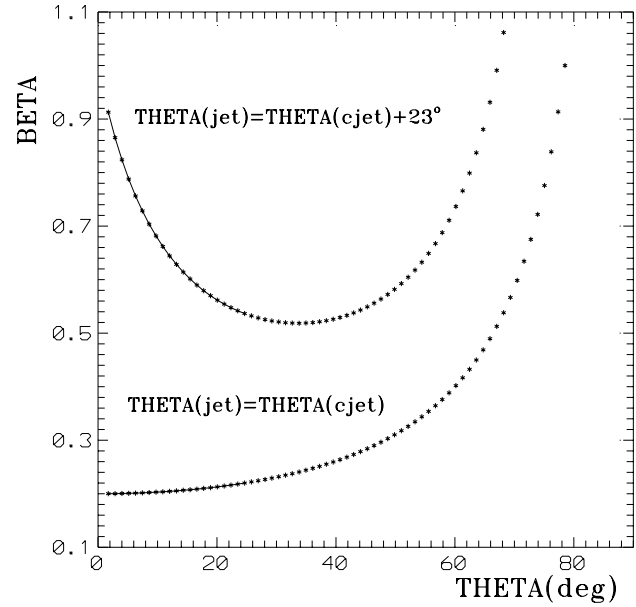


Fig. 3. The jet velocity β and the angle to line of sight θ relations for $\beta_{jet} = \beta_{cjet}$ and $\theta_{jet} = \theta_{cjet}$ (lower line) and $\theta(jet) = \theta(cjet) + 23^\circ$ (upper line)

ened SE lobe toward a core as well as a hot spot midway through the NW lobe and off axis with respect to emission preceding and following it. There is less depolarization on the (NW) jet side (Garrington et al., 1988).

3C 275.1, the FR II-type quasar having $LAS=17''$ at 5GHz, is variable in radio and optical spectral regions. The SE lobe is brighter than NW one at low frequencies and fainter at high ones (Stocke et al., 1985), while the NW lobe is more distant from the core than the SE one.

3.1. Jet velocity and orientation

The ratio of the distances between the radio core and the brightest feature in each radio lobe is defined by:

$$Q = \left(\frac{\theta_{NW}}{\theta_{SE}} \right) = \left(\frac{\theta_j}{\theta_{cj}} \right).$$

At 5 GHz it is equal to 1.50. We adopt a kinematical model of the radio source, in which two plasma streams are ejected from the active core with velocities $V = \beta \cdot c$ in two opposite directions at angle θ to the line of sight. Then, the ratio Q is given by:

$$Q = \left(\frac{1 + \beta \cdot \cos \theta}{1 - \beta \cdot \cos \theta} \right).$$

The value of $Q=1.5$ implies $\beta \cos \theta = 0.2$. The relation between jet velocity β and the angle to the line of sight θ for the observed Q is shown in Fig. 3 (lower line).

It is worth noting that 3C 275.1 is observed at $\theta \geq 50^\circ$ for ejection velocities larger than 0.3 c . In general, the jet and counter-jet might be ejected with different velocities and at different angles to the line of sight, although the probability is quite low (Saikia, 1991). In this case, we have:

$$Q = \left(\frac{1 + \beta \cdot \cos \theta_{cjet}}{1 - \beta \cdot \cos \theta_{jet}} \right) \cdot \left(\frac{\sin \theta_{jet}}{\sin \theta_{cjet}} \right).$$

If we assume that the non-collinearity of the radio structure of 3C 275.1 is due to different ejection angles, then the β - θ relation will have a minimum for $\beta \approx 0.5$ at $\theta \approx (30 \div 40)^\circ$ (upper line in Fig. 3). However, it seems more probable that the deflection of the SE lobe (of about 23°) is due to local density or pressure enhancement than motion of the radio galaxy through the intergalactic or intra-cluster medium (see the Table – $\Delta V_r = -39 \text{ km s}^{-1}$) (Parma et al., 1993). The candidate for localized deflectors might be the gaseous halo and/or the interstellar medium of galaxies in the immediate vicinity of the QSO. If the non-collinearity of the radio structure of 3C 275.1 results from asymmetry of the density of ISM/ICM gas then $Q = 1.50 = \left(\frac{L_1}{L_2} \cdot \frac{\rho_2}{\rho_1}\right)^{0.25}$; where L_1 and L_2 are the radio luminosities of radio lobes; ρ_1 and ρ_2 – the ISM/ICM gas densities in the vicinity of radio lobes. Putting $L_1 = 4.4 \cdot 10^{43} \text{ erg s}^{-1}$ and $L_2 = 1.0 \cdot 10^{44} \text{ erg s}^{-1}$ as given by Strom and Conway (1985) one estimates the ratio of the ISM/ICM gas densities equal to 11.5. We consider that the jet plasma ejected from the core toward the SE lobe exhibits an oblique shock at the interface with the halo of the neighbouring galaxy (galaxy „381” in Table 1) leading to the observed non-collinearity. Furthermore, the observed ratio R of the integrated flux densities S of jet and counter-jet is given by:

$$R = \left(\frac{S_j}{S_{c_j}}\right) = \left(\frac{1+\beta \cdot \cos \theta}{1-\beta \cdot \cos \theta}\right)^{n+\alpha_{av}},$$

where α_{av} is the average spectral index of jet and counter-jet. The index „n” depends upon the ejection model and $n=2$ stands for continuous ejection. However, 3C 275.1 being a lobe-dominated quasar has only a weak jet ($S_j(5 \text{ GHz}) = 0.008 \text{ Jy}$), with no sign of a counter-jet. Therefore, to derive the ratio R we have used lobes instead of jet and counter-jet. $R = \left(\frac{S_{NW}}{S_{SE}}\right)$, changes from 0.44 to 1.30 at 0.408 and 5 GHz respectively. Accordingly, the spectral indices of lobes vary from $\alpha_{0.408}^{1.4} = 0.56$ and 0.94 to $\alpha_{1.4}^5 = 0.72$ and 1.23 for the NW and SE lobes respectively. The SE lobe dominates at low frequencies, i.e. it contains many low energy electrons.

On the other hand, non-visibility of the counter-jet implies $R \geq 4$. Putting $R = 4$ one derives slightly larger values of β for the given angle Θ . In general, our limitation upon $\beta \cos \Theta$ calculated from Q has been confirmed by the ratio R .

We have analysed if the drag force due to the motion of the host galaxy of 3C 275.1 with velocity of $\Delta V_r = 39 \text{ km} \cdot \text{s}^{-1}$ through ICM could cause the bending of the radio jet. We derived the pressure gradient P_r as a sum of the buoyancy pressure gradient of the ICM gas P_b and the dynamic pressure gradient caused by slow galaxy motion P_g , namely $P_r = P_b + P_g$. We have:

$$P_b = 3 \cdot \beta_r \cdot n_o \cdot \frac{r}{a_c^2} \cdot \left(1 + \left(\frac{r}{a_c}\right)^2\right)^{-(1.5 \cdot \beta_r + 1)} \text{ and } P_g = m_p \cdot n_o \cdot \left(1 + \left(\frac{r}{a_c}\right)^2\right)^{-1.5 \cdot \beta_r} \cdot \frac{(\Delta V_r)^2}{R_i}$$

m_p , a_c , β_r , n_o have been defined in Sect. 2. ΔV_r is the velocity of host galaxy in respect to the mean velocity of the cluster. For R_i one might take the size of the host galaxy or the size of the tail or lobe. We have considered both these cases. In the first case we assumed $R_i = 35.4 \text{ kpc}$, while in the second one $R_i = 3.72 \text{ kpc}$, which corresponds to the size of the SE

lobe. We discussed two following cases:

- i) $a_c = 150 \text{ kpc}$; $n_o = 2.6 \cdot 10^{-2} \text{ cm}^{-3}$ and $\rho_{ICM} = 4.35 \cdot 10^{-26} \text{ g} \cdot \text{cm}^{-3}$;
- ii) $a_c = 223 \text{ kpc}$; $n_o = 1.43 \cdot 10^{-2} \text{ cm}^{-3}$.

We obtained the buoyancy pressure gradients about an order of magnitude lower than those due to galaxy motion through ICM. The whole ram pressure gradient changes only slightly between both these cases. At the distance of SE lobe it is equal to about $1.2 \cdot 10^{-36} \text{ dyn} \cdot \text{cm}^{-2} \text{cm}^{-1}$, while the ram pressure due to the motion of radio plasma in SE lobe is larger than $(10^{-32} \div 10^{-34}) \text{ dyn} \cdot \text{cm}^{-2} \text{cm}^{-1}$ for the minimum pressure of the SE lobe, namely from a few 10^{-9} up to a few $10^{-11} \text{ dyn} \cdot \text{cm}^{-2}$. Therefore, it is higher than that due to the motion of the host galaxy through ICM and due to buoyancy effects at least by two orders of magnitude. Accordingly, the non-linear radio structure of the quasar cannot result from the galaxy motion. We suggest that the oblique shock of the plasma jet at the interface with the halo of the neighbouring galaxy or with the cloud of ionized gas in NELR might explain the non-collinearity of radio structure.

3.2. Non-relativistic oblique shock

The solid angle as seen from the core of 3C 275.1 covered by the companion galaxy with a gaseous halo of radius r_g , which is located at a distance R_g from the core is:

$$\Omega_g = 2\pi \left(1 - \left(1 + \left(\frac{r_g}{R_g}\right)^2\right)^{-0.5}\right).$$

The radius of the gaseous halo of a galaxy depends on morphological type and evolutionary effects such as cannibalism and stripping. Hence, the magnitude of r_g is highly uncertain. Putting the radius of the R-image of galaxy „381” – $r_g \approx (2.5 - 3)''$ and $R_g \equiv d = 6.7''$ (see Table 1), we derive $\Omega_g = (0.40 \div 0.55) \text{ sr}$. On the other hand, the solid angle occupied by the SE radio lobe is

$$\Omega_l = 2\pi \left(1 - \left(1 + \left(\frac{r_l}{R_{cl}}\right)^2\right)^{-0.5}\right),$$

where r_l is the radius of the SE radio lobe, i.e. $1.5''$ and R_{cl} is the distance of the SE radio lobe from the compact component, namely $6''$. Hence, $\Omega_l = 0.19 \text{ sr}$. Therefore, the size of the solid angle seen from the core over which deflection by the companion galaxy „381” can occur is $\Omega_d = \Omega_g + \Omega_l = (0.59 \div 0.74) \text{ sr}$. Accordingly, the inelastic collision of the radio jet with the halo of neighbouring galaxy may occur. However, the true distances can differ significantly from the projected ones. One might derive the luminosity distances, the comoving distances and the angular diameter distances. We used the last ones „R” to estimate the projection angles. For the projection angle ζ , the real distance of the galaxy from the quasar core is $R = \frac{R_g}{\cos \zeta}$, while the radius of the spherical galaxy does not change. Taking the distances „R” and „ R_g ” given in Table 1, we obtain that the projection angle might change from 50 to 88° . The accuracy of derived projection angle is about (50-60) %. Thereafter, for $\zeta = 80^\circ$ one calculates $R = 5.76 R_g$, i.e. 38.59 arcsec or about $287 \cdot h^{-1} \text{ kpc}$ and 34.55 arcsec or about $257 \cdot h^{-1} \text{ kpc}$ for the distances of galaxy 381 and SE lobe respectively. For $\zeta = 50^\circ$, we have $R = 1.56 \cdot R_g$, i.e. 10.45 arcsec (78 kpc) and 9.36 arcsec (70

kpc) respectively. Putting these values into above expressions we obtain smaller solid angles. For projection angle $\zeta = 50^\circ$, we have $\Omega_g = 0.25$ sr (for $r_g = 3''$), $\Omega_l = 0.08$ sr, $\Omega_d = 0.33$ sr and the probability of interaction of about 5 %.. For larger projection angles the solid angles are even smaller and the probability of the interaction of the galaxy and the plasma jet is very low. However, the projected positions of the discussed galaxies (see PA in Table 1) are contained within one hemisphere. If we take the impact parameter of about 0.5 Mpc, three galaxies might interact with the radio plasma and probability increases to about 15 %. The other possibility is that the knots emitting narrow-emission lines might be deflectors.

Then, the deflected SE lobe is seen closer to the core because its outward velocity is reduced by deflection. Moreover, its transverse radius is greater than that of the undeflected NW lobe due to internal heating from shock, as observed in 3C 275.1. Therefore, the plasma jet characterized by the jet velocity V_1 , density ρ_1 , Mach number M_1 exhibits the oblique internal shock at the interface with the halo of the neighbouring galaxy or knots emitting narrow lines characterized by density ρ_2 and pressure p_2 . Taking the radius of galaxy „381” equal to 22 kpc ($3''$) and mass $m \approx (1.0 \cdot 10^{11} \div 5.3 \cdot 10^{11})M_\odot$, one derives the average density $\rho_2 = (1.5 \div 7.5) \cdot 10^{-25} \text{gcm}^{-3}$, while for knots the critical density calculated in previous section is about $3.84 \cdot 10^{-24} \text{gcm}^{-3}$. We shall consider classical and relativistic oblique internal shocks since the discussion of the relativistic bulk motion of the emitting plasma in the nuclei of about one hundred radio sources by Ghisellini et al. (1993) indicates that the lobe-dominated QSOs have small Doppler factors (≈ 1), Lorentz factors of the order of 10 and average viewing angles of 25° ($15^\circ \lesssim \Theta \lesssim 30^\circ$).

Firstly, we shall discuss the non-relativistic shock of the initially supersonic jet ($M_1 \geq 1$). The jet exhibits an oblique shock at the interface to the halo of the neighbouring galaxy „y” and bends (see Fig. 4). Subscripts '1' and '2' denote the state of gas upstream of and following the shock (downstream) respectively.

Let η be the deflection angle or the angle by which the velocity vector turns after passage through the shock front and τ the angle that the shock front makes with respect to the velocity V_1 in the flow plane. Neglecting projection effects η is equal to about 23° . The pressure balance is maintained across the bend (shock) interface and the bend moves in the direction of the initial jet velocity with velocity W . In the rest frame of the bend (shock), the flow may be considered as steady. Then we have: $\tan \eta = (\frac{V_1}{W})$. The relations between the post-shock Mach number M_2 , the initial flow Mach number M_1 , the shock inclination angle τ and the deflection angle η for a given value of Γ are, as follows:

$$\cot \eta = \tan \tau \cdot \frac{M_1^2 \cdot (\Gamma + 1)}{2 \cdot (M_1^2 \cdot \sin^2 \tau - 1)} - 1$$

$$M_2^2 = \left(\frac{M_1^2 \cdot (\Gamma - 1)}{2 \cdot \Gamma \cdot (M_1^2 \sin^2 \tau - 1)} \right) + \left(\frac{2 \cdot \cos^2 \tau}{(\Gamma - 1) \cdot \sin^2 \tau} \right).$$

Here Γ is the adiabatic index. These relations are fulfilled for values of τ larger than Mach angles $\alpha = \arcsin(\frac{1}{M_1})$. We

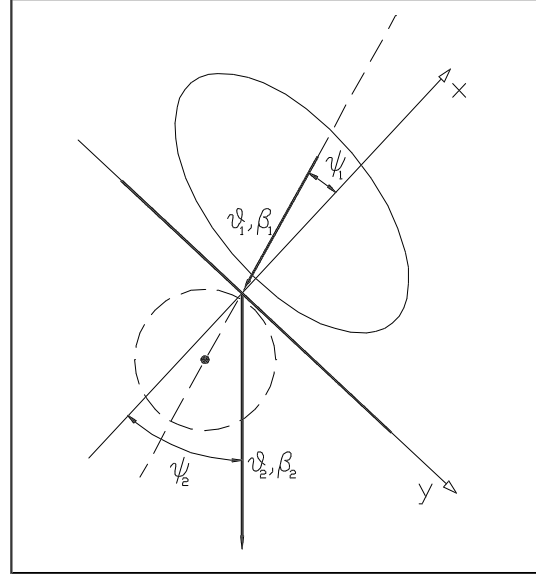


Fig. 4. The schematic picture of the oblique shock in 3C 275.1. The ellipse presents the R-image of the host galaxy of 3C 275.1, while the circle corresponds to the R-image of the neighboring galaxy „381”

have calculated the relation $\eta(\tau)$ for $\Gamma = \frac{5}{3}$ and different values of initial Mach number M_1 . We found the single values of τ , i.e. $\tau \approx 81^\circ$ for initial Mach numbers smaller than about 2.5. For larger initial Mach numbers and $\eta = 23^\circ$ two values of τ are possible, namely $\tau \approx 32^\circ$ for supersonic downstream flow and $\tau \approx 81^\circ$ for sub-sonic downstream flow. On the other hand, the pressure, density and temperature before and after the shock are described by Rankine-Hugoniot relations derived directly from the Euler, energy conservation and state equations. Then, the pressure ratio is given by:

$$\frac{p_2}{p_1} = 2 \cdot \frac{\Gamma}{(\Gamma + 1)} \cdot M_1^2 \cdot \sin^2 \tau - \frac{\Gamma - 1}{\Gamma + 1}.$$

Therefore, for the observed ratio $\frac{p_2}{p_1} = \frac{p_{\min}(SElobe)}{p_{\min}(NWlobe)} = 1.6$, $\Gamma = \frac{5}{3}$ and $\eta = 23^\circ$, one derives $M_1 \cdot \sin \tau \geq 1.22$ and the limitation for the initial Mach number $M_1 \geq 1.22$. The observed initial Mach numbers M_1 are larger than 8 (Strom & Conway, 1985). On the other hand, Wellman et al. (1997) determined the Mach numbers of lobe advance larger than 3. Thereafter, M_2 seems to be supersonic and M_1 might be larger than 8 and $\tau \approx 32^\circ$. Stronger shocks are likely to be associated with more powerful jets and more compressive shocks would produce flatter spectra.

3.3. Relativistic oblique shock

We assumed the structure of the shock, as follows: the x-axis is normal to the shock and the y-axis is in the plane of the shock. The particle acceleration and field amplification occur at the shock. Hence, the emission is dominated by the post-shock region. In general, for the oblique shock the components of the magnetic field are not vanishing. Hence, we have considered the magnetic field in the momentum and energy conservation

equations. We assume that the motion is planar and the velocity and the magnetic field are in plane (x,y) on either side of the discontinuity. The tangential components of velocity are continuous at the surface of discontinuity, i.e. $\beta_{1y} = \beta_{2y}$. Moreover, we take such a coordinate system that the components of the electric field vanish. We consider two cases:

i) the magnetic field is parallel to flow velocities in both upstream and downstream flows. We have:

$$\begin{aligned} \mathbf{v}_1 \times \mathbf{B}_1 &= 0 \\ \text{and} \\ \mathbf{v}_2 \times \mathbf{B}_2 &= 0. \end{aligned}$$

Such assumption gives the relations:

$$v_{1x} \cdot B_{1y} = v_{1y} \cdot B_{1x} \text{ and } v_{2x} \cdot B_{2y} = v_{2y} \cdot B_{2x}.$$

Since the parallel components of shock velocity are preserved, we have $\beta_{1y} = \beta_{2y}$. It gives the relation:

$$\frac{\beta_{1x}}{\beta_{2x}} = \frac{B_{1x}}{B_{2x}} \cdot \frac{B_{2y}}{B_{1y}}.$$

ii) the magnetic field of the upstream flow is parallel to the velocity flow, i.e. $(\mathbf{v}_1 \times \mathbf{B}_1) = 0$, while that of the downstream flow is perpendicular, namely $(\mathbf{v}_2 \cdot \mathbf{B}_2) = 0$. Since the polarization observations of 3C 275.1 by Liu and Pooley (1990) indicate that the magnetic field of the SE lobe is most probably perpendicular or complex, this case seems to be more realistic one. Then one has

$$\beta_{2x} \cdot B_{2y} = -\beta_{2y} \cdot B_{2x}.$$

In both above discussed cases, the number density of particle n_i is conserved. Hence, one has:

$$n_1 \cdot \gamma_1 \cdot \beta_1 = n_2 \cdot \gamma_2 \cdot \beta_2$$

To derive the conservation equations we used the energy-momentum tensor given by:

$$T_k^i = (w + \frac{B^2}{4\pi}) \cdot u^i \cdot u_k - (p + \frac{B^2}{8\pi}) \cdot \delta_k^i.$$

Here $w = e + p$ is the relativistic enthalpy, e - internal energy and $\frac{B^2}{8\pi}$ - the pressure of the magnetic field. Hence, the conservation equations, namely the conservation of the energy and momentum, describe the boundary (jump) conditions. They are as follows:

$$w_1 \cdot \gamma_1^2 \cdot \beta_{1x} = w_2 \cdot \gamma_2^2 \cdot \beta_{2x}$$

$$w_1 \cdot \gamma_1^2 \cdot \beta_{1x}^2 + p_1 + \frac{B_1^2}{8\pi} = w_2 \cdot \gamma_2^2 \cdot \beta_{2x}^2 + p_2 + \frac{B_2^2}{8\pi}$$

$$w_1 \cdot \gamma_1^2 \cdot \beta_{1x} \cdot \beta_{1y} - \frac{1}{4\pi} \cdot B_{1x} \cdot B_{1y} =$$

$$w_2 \cdot \gamma_2^2 \cdot \beta_{2x} \beta_{2y} - \frac{1}{4\pi} \cdot B_{2x} \cdot B_{2y}.$$

For case ii), after the inclusion of perpendicularity of magnetic field condition, one has:

$$w_1 \cdot \gamma_1^2 \cdot \beta_{1x} \cdot \beta_{1y} - \frac{1}{4\pi} \cdot \frac{\beta_{1x}}{\beta_{1y}} \cdot B_{1y}^2 =$$

$$w_2 \cdot \gamma_2^2 \cdot \beta_{2x} \beta_{2y} + \frac{1}{4\pi} \cdot \frac{\beta_{2y}}{\beta_{2x}} \cdot B_{2y}^2$$

The angles of upstream and downstream flow velocities to the shock normal are related by:

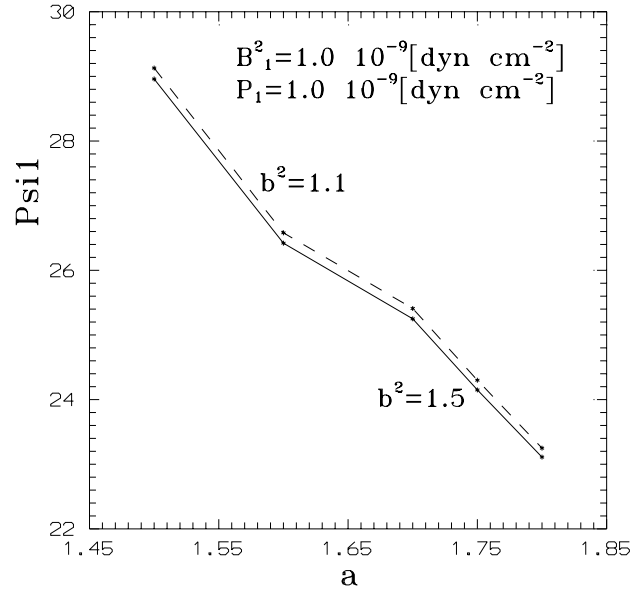


Fig. 5. The changes of ψ_1 with the ratios of the gas „a” and of magnetic „b²” pressures for $\frac{B_1^2}{8\pi} = 1.0 \cdot 10^{-10} \text{ dyn cm}^{-2}$ and $p_1 = 1.0 \cdot 10^{-9} \text{ dyn cm}^{-2}$. $b^2 = 1.4$ (solid line); $b^2 = 1.1$ (dashed line).

$$\tan \psi_2 = \left(\frac{\beta_{1x}}{\beta_{2x}} \right) \cdot \tan \psi_1$$

and

$$\tan \psi_2 = \left(\frac{\beta_{1x}}{\beta_{2x}} \right) \cdot \tan\left(\psi_1 + \frac{\pi}{2}\right)$$

for cases i) and ii) respectively.

We have derived in Appendix B expressions for the velocity components of the gas in the observer’s frame as well as for the angles of upstream and downstream flow velocities for the ultrarelativistic equation of state, i.e. $p_i = \frac{e_i}{3}$.

Knowing the ratio „a” and „b” one might derive the values of other physical parameters for different shock β and different angles between fluid and shock normal.

However, it is seen in Fig. 4, that the angle ψ_2 is equal to $(\psi_1 + \psi_o)$ in the projection on the (x,y) plane. Here ψ_o corresponds to the deflection angle. Hence,

$$\tan \psi_2 = \tan(\psi_1 + \psi_o)$$

and

$$\tan \psi_2 = \frac{\tan \psi_1 + \tan \psi_o}{1 - \tan \psi_1 \cdot \tan \psi_o}.$$

Therefore, from the above relation one derives the changes of the angle ψ_1 with the ratios of the gas „a” and of magnetic field „b²” pressures for values of p_1 from $1.0 \cdot 10^{-13}$ to $1.0 \cdot 10^{-9} \text{ dyn cm}^{-2}$ and of $\frac{B_1^2}{8\pi}$ from $1.0 \cdot 10^{-14}$ to $1.0 \cdot 10^{-9} \text{ dyn cm}^{-2}$. We realized that the values of ψ_1 change only slightly with the value of upstream magnetic pressure and the ratios of magnetic pressures „b²”. On the other hand, the angle ψ_1 depends significantly upon the values of the ratio of gas pressures „a”. It changes from about 20° up to $\approx 40^\circ$ for „a” from 1.1 to 1.9 and for $b^2 = 1.2$, $p_1 = 1.0 \cdot 10^{-9} \text{ dyn cm}^{-2}$ and $\frac{B_1^2}{8\pi} = 1.0 \cdot 10^{-10} \text{ dyn cm}^{-2}$. For an example the changes of ψ_1 with „a” and „b” are shown in Fig. 5.

There is a serious problem, how one might determine the ratios of the magnetic field pressures and of the gas (plasma) ones in upstream and downstream flows. There are a few possibilities for estimation of the gas pressure ratio. We used the following methods:

i) the minimum pressures, i.e.

$$p_{min} = \left(\frac{7}{12}\right) \cdot \left(\frac{1}{2\pi}\right)^{\frac{3}{7}} \cdot \left(\frac{2 \cdot c_{12} L}{V}\right)^{\frac{4}{7}},$$

calculated from radio observations of NW lobe and SE lobe, correspond to p_1 and p_2 respectively. We put $L_1 = 4.4 \cdot 10^{43}$ erg s⁻¹ and $L_2 = 1.0 \cdot 10^{44}$ erg s⁻¹ (Strom and Conway, 1985). Hence, $a = p_{min}^{SE} / p_{min}^{NW} = 1.6$.

ii) the gas pressure of intra-cluster medium (see Sect. 2).

At the distance of SE lobe we have: $P_g = 1.0 \cdot 10^{-10}$ dyn cm⁻². Recently, Wellman et al. (1997) have determined the density and pressures of the ambient gas in the vicinity of radio lobes assuming that radio lobes are ram-pressure confined by the ambient gas. We compared our ICM gas densities determined for „ β ” model with theirs and found our pressures higher and cooling times shorter. Moreover, ICM gas pressure at a distance of SE lobe is lower by about two orders of magnitude than that derived in previous section for inhomogeneous NELR. Therefore, it seems that the ionized knots radiating in forbidden narrow-emission lines might also be responsible for the oblique shock of radio plasma. Thereafter, the ratio of gas pressures of upstream flow to downstream one might change from 1.6 to 3.3. Therefore, for case i) we have:

$$\tan \psi_2 = \left(\frac{5.8 \div 10.9}{4.6 \div 6.3}\right) \cdot \tan \psi_1.$$

On the other hand, for deflection of the upstream flow by the angle $\psi_o = 23^\circ$ the ratio „a” should be larger than about 4. For a=4, one derived $\psi_1 \approx 34^\circ$.

There is no reliable estimations of the magnetic field in 3C 275.1. Basing upon the MERLIN observations of polarization at 18 cm Liu and Pooley (1990) have given the general discussion of the magnetic field. According to Strom and Conway (1985) the strengths of observed magnetic field are $B_1 = 150 \mu G$ and $B_2 = 92 \mu G$ for NW and SE lobes respectively. Hence, the magnetic pressures given by $\frac{B^2}{8\pi}$ are equal to $6.7 \cdot 10^{-12}$ and $3.4 \cdot 10^{-12}$ dyn cm⁻² for $\frac{B_1^2}{8\pi}$ and $\frac{B_2^2}{8\pi}$ respectively. They consist only a few percent of gas pressures. However, they are stronger in the parsec scale jets. On the other hand, Liu and Riley (1992) have determined the strengths of magnetic fields as equal to $B_1 = 33 \pm 1 \mu G$ and $B_2 = 40 \pm 2 \mu G$. Hence, we have $b^2 = 1.5 \pm 0.4$. For $b^2 = 1.5$, $P_1 = 1.0 \cdot 10^{-10}$ dyn cm⁻² and $\frac{B_1^2}{8\pi} \approx 1.0 \cdot 10^{-12}$ dyn cm⁻² the angle ψ_1 between the direction of upstream velocity and the surface normal to the shock changes from about 25° up to 48° for „a” from 1.7 to 1.1. Assuming ψ_1 roughly 30° we calculated from the expression given in Appendix B the angle between observer and shock surface $\Delta \approx 56^\circ$. Putting the observed values of parameters, i.e. a=1.6, $b^2 = 1.5$, $P_1 = 1.0 \cdot 10^{-10}$ dyn cm⁻² and $\frac{B_1^2}{8\pi} \approx 1.0 \cdot 10^{-12}$ dyn cm⁻², we obtain from the formula for velocities given in Appendix B, $\beta_{1x} = 1.29 \cdot \gamma_y^{-1}$ and $\beta_{1x} \geq 0.37$. Thereafter, we have $\gamma_y \leq 3.5$

and $\beta_{1y} = \beta_{2y} \leq 0.96$. In summary, one should include the magnetic pressure into the considerations of oblique shock in spite that in kiloparsec jets it consists only a few percent of gas pressures.

4. Conclusions

We considered the dynamics of the groups of galaxies around 3C 275.1. Basing upon criterion „ 3σ ” we realized that only five galaxies from the lists published by Hintzen (1984) and Ellingson and Yee (1994) are dynamically bound with the quasar. It is worth noting that the host galaxy of quasar with its low radial velocity in respect to the group, i.e. -39 km s⁻¹, resides in the bottom of gravitational potential well of the group. Accordingly, its relative motion through the ICM gas cannot explain the non-collinearity of the radio structure of the quasar. We proposed that the oblique shock of radio jet at the interface with the halo of the neighboring galaxy „381” or with knots of ionized gas emitting the forbidden narrow-emission lines might be responsible for the deflection of counter-jet. The knots of the ionized gas can be produced by the cooling flow with the deposition mass rate of the order of $140 M_\odot$ yr⁻¹. Then, the calculated number and mass densities in such knots of the size of 10 kpc are about 2.3 cm⁻³ and about $3.8 \cdot 10^{-24}$ g cm⁻³ respectively. To explain the deflection angle of 23° we consider two cases of oblique shocks. In the first case the flow velocities and the magnetic fields are parallel to each other in upstream and downstream flows, while in the second one the magnetic field become perpendicular to flow velocities after the shock. We derived the relation between the angle ψ_2 and the angle between the upstream flow velocity ψ_1 and the normal to the discontinuity surface as the functions of the ratios of gas „a” and of magnetic „b²” pressures. For observed ratios of magnetic field pressures $b^2 = 1.5$, of gas pressures a=1.6, the upstream gas pressure $P_1 = 1.0 \cdot 10^{-10}$ dyn cm⁻² and $\frac{B_1^2}{8\pi} = 1.0 \cdot 10^{-12}$ dyn cm⁻² we derived the angles between the upstream velocity and normal to surface shock ψ_1 and between the surface shock and the line of sight Δ equal to $\approx 30^\circ$ and $\approx 56^\circ$ respectively. We also calculated the conditions for upstream velocity $\beta_{1x} \geq 0.37$ and $\gamma_y \leq 3.5$.

Acknowledgements. We would like to thank Andrzej Marecki for very careful and critical reading of the manuscript.

We thank Maria Rioja for the data correlation.

We thank also Fredrik T Rantakyro and Hardip Sanghera for important suggestions and help in calibrating of amplitudes of the EVN data.

We are particularly grateful Dr Strom for valuable comments on the manuscript.

Appendix A: See Table A1

Appendix B

We derive the expressions for the velocity components and deflection angles for two above discussed cases:

i) the magnetic field is parallel to flow velocities in both upstream and downstream flows

Table A1. Fluxies of 3C 275.1 at different frequencies - references

Number	Frequency [MHz]	Flux [Jy]	Ref.
1	38	43.51*	39, Kellermann 1969
2	80	41.00*	66, Slee 1973
3	160	15.90*	67, Slee 1977
4	178	17.30*	52, Pilkington 1965
5	178	18.30	6, Barthel 1989
6	178	16.66*	76, Veron 1977
7	318	10.71*	14, Condon 1994
8	408	8.30*	18, Ekers 1969
9	408	7.55	71, Stocke 1985
10	609	6.29	74, Strom 1985
11	635	6.67*	79, Wills 1975
12	750	5.34*	51, Pauliny-Toth 1966
13	750	5.00*	39, Kellermann 1969
14	1400	2.81	80, Witzel 1971
15	1400	2.95*	70, Stocke 1969
16	1400	2.90*	39, Kellermann 1969
17	1400	2.73	46, Liu 1992
18	1400	2.95	42, Laing 1980
19	1410	3.08*	79, Wills 1975
20	1600	1.60	2, Akujor 1994
21	2650	1.67*	79, Wills 1975
22	2695	1.58*	77, Veron 1991
23	2695	1.60*	1, Adgie 1972
24	2700	1.66*	79, Wills 1975
25	2700	1.60*	39, Kellermann 1969
26	4866	0.90	71, Stocke 1985
27	5000	1.05	37, Jenkins 1977
28	5000	1.01	46, Liu 1992
29	5000	1.00	47, Milton 1970
30	5000	0.90	42, Laing 1980
31	5000	0.91*	77, Veron 1991
32	5000	0.90*	39, Kellermann 1969
33	5009	1.16*	64, Shimmins 1969
34	5009	0.98*	65, Shimmins 1973
35	10695	0.77*	40, Kellermann 1973
36	14900	0.52*	26, Genzel 1976
37	15000	0.39	56, Riley 1978
38	15000	0.58	10, Borger 1985

From the boundary conditions, we obtain the following relations for the velocity components:

$$\beta_{1x} = \frac{\gamma_2}{\gamma_1} \cdot \left[\frac{w_2}{w_1} \cdot \frac{A}{w_2 \cdot \gamma_2^2 - w_1 \cdot \gamma_1^2} \right]^{0.5}$$

$$\beta_{2x} = \frac{\gamma_1}{\gamma_2} \cdot \left[\frac{w_1}{w_2} \cdot \frac{A}{w_2 \cdot \gamma_2^2 - w_1 \cdot \gamma_1^2} \right]^{0.5}$$

Here:

$$A = (p_2 - p_1) + \frac{1}{8 \cdot \pi} \cdot (B_{2y}^2 - B_{1y}^2); \quad w_1 = e_1 + p_1 \text{ and } w_2 = e_2 + p_2.$$

Putting $a = \frac{p_2}{p_1}$ and $b^2 = \frac{B_2^2}{B_1^2}$ as the ratios of gas and of magnetic field pressures respectively, we derive:

$$A = p_1 \cdot (a - 1) + \frac{B_1^2}{8 \cdot \pi} \cdot (b^2 \cdot \sin^2 \psi_2 - \sin^2 \psi_1).$$

The Lorentz factors are described by: $\gamma_i = (1 - (\beta_{ix}^2 + \beta_{iy}^2))^{-0.5}$. Since $\beta_{1y} = \beta_{2y}$ the normal components of upstream and downstream velocities are related to Lorentz factors by:

$$\beta_{1x}^2 - \beta_{2x}^2 = \frac{\gamma_1^2 - \gamma_2^2}{\gamma_1^2 \cdot \gamma_2^2}.$$

Applying the Lorentz transformation to above expressions and putting w_1 and w_2 , one has after the calculations:

$$\beta_{1x} = \gamma_y^{-1} \cdot \left(\frac{(e_2 + p_1) \cdot A}{(e_1 + p_2) \cdot (e_2 - e_1)} \right)^{0.5}$$

$$\beta_{2x} = \gamma_y^{-1} \cdot \left(\frac{(e_1 + p_2) \cdot A}{(e_2 + p_1) \cdot (e_2 - e_1)} \right)^{0.5}$$

Here $\gamma_y = (1 - \beta_y^2)^{-0.5}$ is the Lorentz factor corresponding to the y - component of velocity. The above expressions reduce to those ones given by Bicknell (1994: see also Landau and Lifshitz, 1987) for $B_1 = B_2 = 0$. Putting the above expressions for β_{1x} and β_{2x} , one has:

$$\tan \psi_2 = \left(\frac{3 \cdot a + 1}{3 + a} \right) \cdot \tan \psi_1$$

The above relations can be Lorentz transformed to the observer's frame. For an example:

$$\gamma_{fl,obs} = \gamma_{sh} \cdot \gamma_{fl,sh} \cdot (1 + \beta_{sh} \cdot \beta_{fl,sh}),$$

where β_{sh} and γ_{sh} refer to the shock; subscripts „fl,obs” and „fl,sh” refer to fluid with respect to observer and fluid with respect to shock respectively. Accordingly, the velocity components of the gas in the observer's frame for the ultra-relativistic equation of state, i.e. $p_i = \frac{e_i}{3}$ and $w_i = 4 \cdot p_i$, are given by:

$$\beta_{1x}^{obs} = \gamma_{y,fl,obs}^{-1} \cdot \left(\frac{(3a+1) \cdot A}{3 \cdot (3+a) \cdot (a-1)} \right)^{0.5}$$

$$\beta_{2x}^{obs} = \gamma_{y,fl,obs}^{-1} \cdot \left(\frac{(a+3) \cdot A}{3 \cdot (1+3 \cdot a) \cdot (a-1)} \right)^{0.5}$$

ii) the magnetic field of the upstream flow is parallel to the velocity flow, while that of downstream flow is perpendicular. We derive from the above given jump (shock) conditions the expressions for the normal components of upstream and downstream flow velocities, as follows:

$$\beta_{1x} = \frac{\gamma_2}{\gamma_1} \cdot \left[\frac{A}{w_1 \cdot \gamma_2^2 - w_2 \cdot \gamma_1^2 \cdot S^2} \right]^{0.5};$$

$$\beta_{2x} = \frac{\gamma_1}{\gamma_2} \cdot S \cdot \left[\frac{A}{w_1 \cdot \gamma_2^2 - w_2 \cdot \gamma_1^2 \cdot S^2} \right]^{0.5};$$

$$\beta_{2y} = B_{1y} \cdot$$

$$\left[\frac{1}{4 \cdot \pi} \cdot \frac{A \cdot S}{\gamma_1^2 \cdot A \cdot S \cdot (w_1 - w_2 \cdot S) - \frac{1}{4 \cdot \pi} \cdot B_{2y}^2 \cdot (w_1 \cdot \gamma_2^2 - w_2 \cdot \gamma_1^2 \cdot S^2)} \right]^{0.5};$$

where: $B_{1y} = B_1 \cdot \sin \psi_1$ and $B_{2y} = B_2 \cdot \cos \psi_2$.

Accordingly, one has:

$$\beta_{2x} = \frac{\gamma_2^2}{\gamma_2} \cdot S \cdot \beta_{1x}. \text{ Here: } S = \frac{w_1 + \frac{B_1^2}{4\pi}}{w_2 + \frac{B_2^2}{4\pi}}$$

and the compression ratio of shock for gas is given by:

$A = p_1 \cdot (a - 1) + \frac{B_1^2}{8\pi} \cdot (b^2 \cdot \cos^2 \psi_2 - \sin^2 \psi_1)$. Due to interaction of the magnetic field and of plasma flow there are the different Lorentz factors for normal components of velocities β_x , i.e. $\gamma_x = (1 - \beta_x^2)^{-0.5}$, and for those of magnetic field, namely

$$\gamma_B = \left(1 - \frac{\beta_x^2}{\sin^2 \psi_2}\right)^{-0.5}.$$

The laboratory and rest frame variables are related via the Lorentz transformation of mass density $\gamma \cdot n$, of momentum density $\gamma^2 \cdot w \cdot \beta$ and of energy density $\gamma^2 \cdot w - p$. Moreover, the angle Θ between the jet direction and the observer (the line of sight), discussed in the beginning of this section, is related to the angle between normal to the shock surface and the line of sight Θ_1 and to the angle between observer and the shock surface Δ by:

$$\cos \Theta = \cos \psi_1 \cdot \cos \Theta_1 + \sin \psi_1 \cdot \sin \Theta_1 \cdot \cos \Delta.$$

Applying the Lorentz transformation to above solutions, we derive for the ultrarelativistic equation of state the expressions:

$$\beta_{1x} = \gamma_y^{-1} \cdot 4 \cdot a \cdot S^2 \cdot \left[\left(\frac{S}{2 \cdot (4 + \frac{A}{p_1}) \cdot (4 + \frac{A}{p_1} - 4 \cdot a \cdot S^2)} \right) \cdot (-G + (G^2 - H)^{0.5}) \right]^{0.5};$$

$$\beta_{2x} = \frac{4 + \frac{A}{p_1}}{4 \cdot a \cdot S^3} \cdot \left[\beta_{1x} - \frac{A}{(4p_1 + A) \cdot \beta_{1x}} \right].$$

Here:

$$S = \frac{16 \cdot \pi \cdot p_1 + B_1^2}{16 \cdot \pi \cdot p_1 \cdot a + B_1^2 \cdot b^2};$$

$$K = \frac{A}{4a \cdot S^2 \cdot (4p_1 + A)} \cdot \left(4 + \frac{A}{p_1} - 4a \cdot S^2 \right) + \left(\frac{A}{4p_1 + A} - 1 \right),$$

$$G = S + 2 \cdot K \cdot \frac{4 + \frac{A}{p_1}}{4 \cdot a \cdot S^3}$$

and

$$H = \frac{1}{16} \cdot \frac{4 + \frac{A}{p_1}}{a^3 \cdot S^8 \cdot p_1} \cdot \left(4 + \frac{A}{p_1} - a \cdot S^2 \right) \cdot A \cdot K.$$

Thereafter, the relation between the angles of the pre- and post-shock velocities to the shock normal is described by:

$$\tan \psi_2 = \frac{32a^3 \cdot S^8 \cdot (-G + (G^2 - H)^{0.5}) \cdot \tan(\psi_1 + \frac{\pi}{2})}{(4 + \frac{A}{p_1}) \cdot \{8 \cdot a^2 \cdot S^5 \cdot [-G + (G^2 - H)^{0.5}] - A \cdot (4 + \frac{A}{p_1} - 4a \cdot S^2)\}}.$$

Appendix C

We suppose that the radio structure of 3C 275.1 is already disturbed at the parsec scale, since there are knots of forbidden line emission from OII and OIII ions in the nucleus of the host galaxy. Hence, we made high resolution observation of the core of 3C 275.1. The VLBI Mk III observation was made in November 16, 1994 at frequency 1.6 GHz with 6 EVN stations: Effelsberg, Jodrell Bank, Medicina, Noto, Onsala and Westerbork. There were significant interferences from GLONASS in this session, and in addition due to some technical problems, almost whole information from baselines with WSRT station was lost. Using the closure phase method (Jennison 1958, Rogstad 1968, Rogers

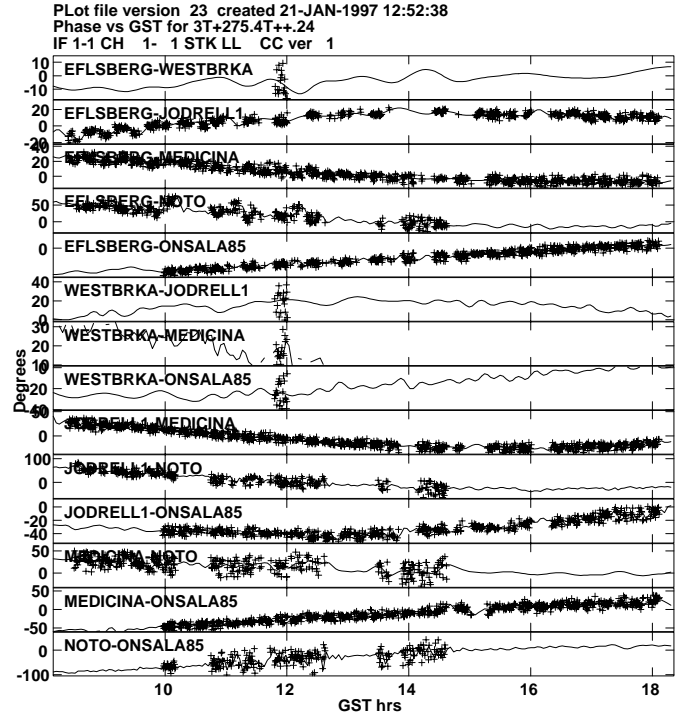


Fig. C1. The phase vs. time for the u-v data used to obtain the „clean” map in Fig. C2. The solid line indicates the model visibilities from the phase-reference map (Fig. C2).

et al. 1974) and CLEAN algorithm in AIPS package (Högbom 1974) to deconvolve the data, we obtained the „clean” map of 3C 275.1 (Fig. C2). There are not significant features at distances above 40 mas from the core (the centre of the map). Probably, the information about it was lost by reason of a very poor u-v coverage of the data. The frequency 1.6 GHz was too low and the baselines too short to resolve the core of the quasar. Fig. C2 shows an elongation of the radio structure at a distance ~ 30 -40 mas from the core with position angle about 255° . It may be the result of interaction between out-flowing plasma of the QSO and the nonuniform ionized gas strongly emitting in forbidden [OII] and [OIII] lines. The contour levels of the elongation are only about 0.5-1 % of the peak. We suggest, that further studies of the milliarcsecond structure of 3C 275.1 leading to resolving the core of the quasar and to confirming the elongation of its radio structure are needed.

References

- Adgie G. et al., 1972, MNRAS 159, 223
- Akujor C. E. et al., 1994, A&A Suppl. 105, 247
- Allen S. W. et al., 1995, MNRAS 275, 741
- Arp H., 1996, A&A 316, 57
- Baars J.W.M., Genzel R., Pauliny-Toth I.I.K., Witzel A., 1977, A&A 61, 99
- Barthel P. D., 1989, ApJ 336, 606
- Beers T.C., Flynn K., Gebhardt K., 1990, AJ 100, 32
- Bicknell G. V., 1994, ApJ 422, 542
- Böhringer H., Fabian A. C. K., 1989, MNRAS 237, 1147

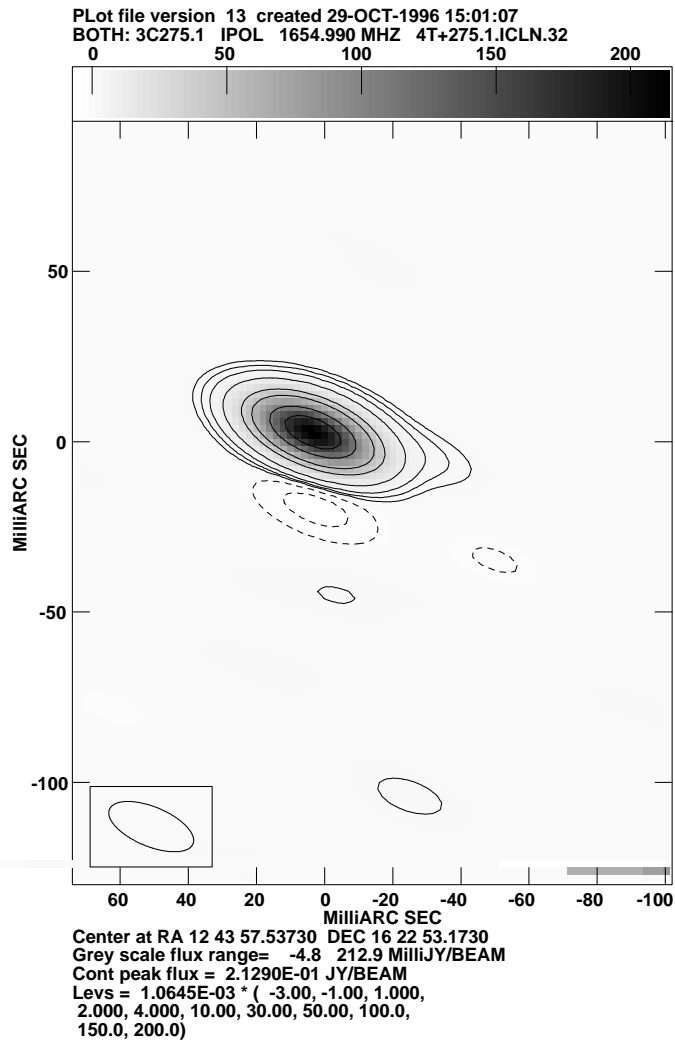


Fig. C2. The „clean” EVN map of 3C 275.1 at frequency 1.6 GHz. The peak of the map is 212.9 mJy/beam. The beam is: 26.53×11.59 mas, P.A. $67^\circ.49$. The contour levels are: dashed: -1.5, -0.5; solid: 0.5, 1, 2, 5, 15, 25, 50, 75 % of the peak.

Bogers W. J. et al., 1985, A&A Suppl. 105, 91
 Boroson T. A., Green R. F., 1992, ApJS 80, 109
 Bremer M. N., Crawford C. S., Fabian A. C., Johnstone R. M., 1992, MNRAS 254, 614
 Chambers K. C., Miley G. K., van Breugel W., 1987, Nature 329, 604
 Condon J. J. et al., 1994, AJ 79, 122D
 Crawford C. S., Fabian A.C., 1989, MNRAS 239, 219
 Crawford C. S., Fabian A.C., George I. M., Naylor T., 1991, MNRAS 248, 139
 Edge A.C., Stewart G.C., 1991, MNRAS 252, 428
 Ekers J. A., 1969, Austr. J. Phys. Suppl. 7, 1
 Ellingson E., Yee H. K. C., 1994, ApJS 92, 33
 Fabian A. C., Crawford C. S., Johnstone R. M., Thomas P. A., 1987, MNRAS 228, 963
 Fabian A. C., Nulsen P. E. J., Canizares C. R., 1984, Nature 310, 733
 Fabian A. C., Nulsen P. E. J., Canizares C. R., 1991, A&AR 2, 191
 Falcke H., Malkan M. A., Biermann P. L., 1995, A&A 298, 375
 Forbes D. A., Crawford C. S., Fabian A.C., Johnstone R. M., 1990, MNRAS 244, 680

Garrington S. T., Leahy J. P., Conway R. G., Laing R. A., 1988, Nature 331, 147
 Genzel R. et al. 1976, AJ 81, 1084
 Ghisellini G., Padovani P., Celotti A., Maraschi L., 1993, ApJ 407, 65
 Heckman T. M. et al., 1989, ApJ 338, 48
 Hes R., Barthel P. D., Fosbury R. A. E., 1993, Nature 362, 326
 Hintzen P., 1984, ApJS 55, 533
 Hintzen P., Boeshaar G. O., Scott J. S., 1981, ApJ 246, L1
 Hintzen P., Stocke J., 1986, ApJ 308, 540
 Högbom J.A., 1974, A&A Suppl. 15, 417
 Hutchings J. B., 1992, AJ 104, 1311
 Jackson N., Browne I. W. A., 1991a, MNRAS 250, 414
 Jackson N., Browne I. W. A., 1991b, MNRAS 250, 422
 Jenkins C. J. et al., 1977, Mem. RAS 84, 61
 Jennison R.C. (1958), MNRAS 118, 276
 Kellermann K. I., et al., 1969, ApJ 157, 1
 Kellermann K. I. et al., 1973, AJ 78, 828
 Kühr et al., 1979, "A Catalogue of Radio Sources", MPIfR, Bonn, Preprint No. 55
 Laing R.A., Peacock J.A., 1980, MNRAS 190, 903
 Laing R.A., 1988, Nature 331, 149
 Landau L. D., Lifsic E.M., 1987, in: "Fluid Mechanics", Oxford Univ. Press, Oxford
 Liu R., Pooley G. G., 1990, MNRAS 245, 17
 Liu R., Pooley G. G., Riley J.M., 1992, MNRAS 257, 545
 Milton S., 1970, MNRAS 149, 101
 Navarro J. F., Frenk C. S., White S. D. M., 1995, MNRAS 275, 720
 Padovani P., Urry C. M., 1992, ApJ 387, 449
 Parma P. et al., 1993, A&A 267, 31
 Pauliny-Toth I. I. K. et al., 1966, ApJ Suppl. 116, 65
 Pilkington J. D. H., et al., 1965, MNRAS 69, 183
 Prestwich A. H. et al., 1995, ApJ 438, L71
 Raymond J. C., Smith B. W., 1977, ApJS 35, 419
 Rector T.A., Stocke J.T., Ellingson E., 1996, AJ (in press)
 Riley J. M., Pooley G. G., 1978, MNRAS 184, 769
 Rogers A.E.E., Hinteregger H.F., Whitney A.R., 1974, ApJ 193, 293
 Rogstad D.H., 1968, Applied Optics, 7, 585
 Saikia D. J., 1991, MNRAS 197, P11
 Sarazin C. L., 1986, Rev. Mod. Phys. 58, 1
 Sarazin C. L., O'Connell R.W., Mc Namara B.R., 1992a, ApJ 389, L59
 Sarazin C. L., O'Connell R.W., Mc Namara B.R., 1992b, ApJ 397, L31
 Schmidt M., Green R.F., 1983, ApJ 269, 352
 Shimmins A. J. et al., 1969, Austr. J. Phys. Astrophys. Suppl. 8, 1
 Shimmins A. J. et al., 1972, Austr. J. Phys. Astrophys. Suppl. 23, 1
 Slee O. B. et al., 1973, Austr.J.Phys.Suppl. 27, 1
 Slee O. B. et al., 1977, Astr.J.Phys.Suppl. 43, 1
 Stewart G. C., Fabian A. C., Jones C., Forman W., 1984, ApJ 285, 1
 Stark A. A. et al., 1992, ApJS 79, 77
 Stocke J. S., 1969, Astr. J Phys. Suppl. 7, 1
 Stocke J. T. et al., 1985, ApJ 299, 799
 Stockton A., MacKenty J. W., 1987, ApJ 316, 584
 Stockton A., 1980, in: IAU Symposium 92, "Objects of High Redshift", ed. G. C. Abell & P. J. E. Peebles, Dordrecht Reidel, p.89
 Strom R.G., Conway R.G., 1985, A&AS 61, 547
 Tananbaum H. et al., 1979, ApJ 230, 540
 Veron P., 1977, A&A Suppl. 30, 131
 Veron P. et al., 1991, ESO Scientific Report No 10
 Wilkes B.J. et al., 1994, ApJS 92, 53
 Wills B. J. et al., 1975, Astr. J. Phys. Astrophys. Suppl. 38, 1
 Witzel A. et al., 1971, A&A 11, 171
 Yahil A., Vidal N.V., 1977, ApJ 214, 347
 Yee H.K.C., Green R.F., 1987, ApJ 319, 28